

Inverse Kinematics for a 6-Degree-of-Freedom Robot Manipulator Using Comprehensive Gröbner Systems

Takumu Okazaki¹, Akira Terui¹[0000–0003–0846–3643], and Masahiko Mikawa¹[0000–0002–2193–3198]

University of Tsukuba, Tsukuba, Japan
 terui@math.tsukuba.ac.jp
 mikawa@slis.tsukuba.ac.jp
<https://researchmap.jp/aterui>

Abstract. We propose an effective method for solving the inverse kinematic problem of a specific model of 6-degree-of-freedom (6-DOF) robot manipulator using computer algebra. It is known that when the rotation axes of *three* consecutive rotational joints of a manipulator intersect at a single point, the inverse kinematics problem can be divided into determining position and orientation. We extend this method to more general manipulators in which the rotational axes of *two* consecutive joints intersect. This extension broadens the class of 6-DOF manipulators for which the inverse kinematics problem can be solved, and is expected to enable more efficient solutions. The inverse kinematic problem is solved using the Comprehensive Gröbner System (CGS) with joint parameters of the robot appearing as parameters in the coefficients to prevent repetitive calculations of the Gröbner bases. The effectiveness of the proposed method is shown by experiments.

Keywords: Comprehensive Gröbner Systems · Robotics · Inverse kinematics · Trajectory planning

1 Introduction

1.1 Problem Statements and Related Work

This paper discusses the motion planning of a 6-Degree-of-Freedom (DOF) robot manipulator. A manipulator is a robot resembling a human hand, consisting of *links* that function as a human arm and *joints* as human joints (see Fig. 2). Each link is connected to the others by a joint. The first link is connected to the ground, and the last link, called the *end-effector*, contains the hand, which can be moved freely. In this paper, we discuss targeting a manipulator called “myCobot 280” [2] (hereafter referred to as “myCobot”). It has six revolute joints, meaning each joint can rotate around its axis. Thus, myCobot has 6-DOF. As its manufacturer describes [2], myCobot has been widely sold for “research and education, science and technology applications, and commercial exhibitions.”

In this paper, we deal with the inverse kinematic problem of the manipulator. The inverse kinematic problem is a problem in finding the joint angles of the robot manipulator corresponding to (or achieving) a given end-effector's position and orientation. In this study, we focus on two main challenges. The first is solving the inverse kinematics problem for a 6-degree-of-freedom (6-DOF) manipulator. The second is improving the efficiency of solving the inverse kinematics problem using Gröbner basis computation.

For the inverse kinematic problem of 6-DOF robot manipulators, several methods have been proposed, including computer algebra [5, 10, 13]. However, solving the inverse kinematics problem for 6-DOF manipulators is often challenging. In particular, algebraic approaches tend to result in large and complex systems. For example, Pieper [17] has reported that, after elimination of variables with algebraic methods, the degree of the resulting univariate equation exceeds 500,000, making it difficult to solve the inverse kinematics problem of a 6-DOF manipulator using algebraic methods in general.

Therefore, previously proposed methods solve the problem by appropriately dividing it into smaller sub-problems, thereby reducing the size of each problem and solving them with a realistic amount of computation [5, 17]. Generally, a 6-DOF manipulator cannot independently determine the orientation and position of the end-effector. Thus, it is difficult to solve the general inverse kinematics problem analytically. *However, if the manipulator includes a spherical joint with 3-dimensional rotation, the orientation and position of the end-effector can be determined independently.* Then, the inverse kinematics problem can be separated into a 3-dimensional problem for orientation and a 3-dimensional problem for position. Furthermore, Pieper [17] has demonstrated that if the rotational axes of three consecutive rotational joints intersect at a single point, the motion of these three joints is kinematically equivalent to a spherical joint. He has proposed a solution to the inverse kinematics problem, focusing on this intersection point. This method was remarkable in solving the inverse kinematics problem for 6-DOF manipulators; however, it also has some limitations. One major drawback is that it cannot be applied unless the rotational axes of three consecutive joints intersect at a single point.

As for Gröbner basis computation, methods by reducing the inverse kinematic problem to a system of polynomial equations and using the Gröbner basis computation have been proposed for several types of robots, including manipulators [3, 6, 13, 20, 23, 24]. Compared to numerical methods, the use of the Gröbner basis computation has advantages, such that it can search for solutions globally so that the number of solutions of the inverse kinematics problem that can be obtained before the actual motion of the manipulator.

On the other hand, a disadvantage of the Gröbner basis computation is the relatively high computational cost compared to numerical methods, especially in the case of trajectory planning. The trajectory planning problem of the manipulator is to determine a sequence of joint configurations that the manipulator should follow to move the end-effector along a specified trajectory. In solving the trajectory planning problem, finitely many points on the trajectory along

the path of the end-effector are given, and then we solve the inverse kinematic problem at each point. When solving a trajectory planning problem, the computational cost of repeatedly calculating the Gröbner basis at each point of the trajectory may become a significant issue.

1.2 Our Previous Approach

We have proposed the following methods for the 3-DOF manipulator’s inverse kinematic and trajectory planning problems. Our first work [16] consists of the following: 1) For the inverse kinematic problem, by using the Comprehensive Gröbner System (CGS) [21] and the real Quantifier Elimination (QE) based on the CGS [4], called the CGS-QE method, we have proposed a method to certify the existence of a solution to the inverse kinematic problem; 2) using this method for trajectory planning, we have proposed an efficient method that prevents the repeated calculation of the Gröbner basis. In a follow-up paper [26], by using the CGS-QE method, we have proposed a method to certify the existence of a solution to the inverse kinematic problem for the whole trajectory given as a line segment.

1.3 Contributions

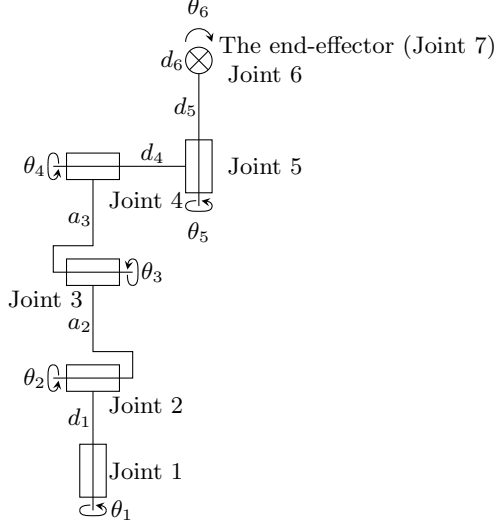
Based on the above results, we propose the following methods for the inverse kinematic problem of a 6-DOF manipulator (myCobot).

We further extend Pieper’s method and propose a solution for the case where the rotational axes of two consecutive joints intersect at a single point, which is applicable to a wider variety of robots. Our method enables us to globally and explicitly determine the solution to the inverse kinematics problem of myCobot, including the joint angles.

Furthermore, we use the CGS for solving a parametric system of polynomial equations, which is important for avoiding recalculating the Gröbner basis in trajectory planning (see Sect. 5). Note that in our experiments, the computation of the CGS has not been fully completed; however, in the experimental results for the inverse kinematics problems constructed by the authors from pre-existing randomly generated joint configurations, the inverse kinematics problems were successfully solved using the partially computed CGS.

1.4 Organization of the Paper

This paper is organized as follows. In Sect. 2, we describe the inverse kinematic problem of myCobot. In Sect. 3, we propose a method to solve the inverse kinematic problem of myCobot using the CGS, and present it in the form of an algorithm. In Sect. 4, we show the effectiveness of the proposed method by experiments. In Sect. 5, we discuss conclusions and future work.

**Fig. 1.** myCobot 280 [2]**Fig. 2.** myCobot with six rotational joints and five links

2 The inverse kinematic problem of myCobot

2.1 Description of MyCobot

myCobot 280 [2] (referred to as “myCobot”, shown in Figure 1) is a 6-DOF robot manipulator with six rotational joints connected in series. The arm length is 350 [mm], and it has a working radius of 280 [mm] centered at a height of approximately 130 [mm] from the ground. myCobot can be controlled using programming languages such as Python, C++, and C#. Additionally, it can be controlled using ROS (Robot Operating System) [9], a standard control environment in robotics. Figure 2 shows a block diagram of myCobot.

2.2 Description of the Transformation Matrix

In the following, we formulate the inverse kinematic problem of myCobot using the Denavit–Hartenberg convention [1] (referred to as “D-H convention”). First, we define the symbols necessary for defining the coordinate systems. Let Σ_i be the coordinate system w.r.t. Joint i , and ${}^i x$, ${}^i y$, and ${}^i z$ be the x , y , and z -axis of Σ_i , respectively. Let \mathcal{O}_i be the origin of Σ_i , and ${}^{i-1}l_i$ be the common normal of the axes ${}^{i-1}z$ and ${}^i z$.

According to the D-H convention, for $i = 1, \dots, 7$, the coordinate system Σ_i is defined as a right-handed coordinate system that satisfies the following: the origin \mathcal{O}_i is placed at Joint i ; the axis ${}^i z$ is aligned with the rotation axis of Joint i , with the positive direction pointing towards Joint $i + 1$; the ${}^i x$ and ${}^i y$ axes follow the conventions of the 3D visualization tool RViz [8] in ROS. Note that Σ_1 is treated as the global coordinate system.

Table 1. Parameters in A_i for the RViz coordinate system in myCobot

Joint	a_i	α_i	d_i	θ_i	δ_i
1	0	$\pi/2$	d_1	θ_1	$-\pi/2$
2	$-a_2$	0	0	θ_2	0
3	$-a_3$	0	0	θ_3	$-\pi/2$
4	0	$\pi/2$	d_4	θ_4	$\pi/2$
5	0	$-\pi/2$	d_5	θ_5	0
6	0	0	d_6	θ_6	0

Next, the transformation matrix from Σ_{i+1} to Σ_i is defined with the following parameters. Note that, for each parameter, the unit of length is expressed in [mm], and the unit of angle is expressed in [rad]. Let a_i be the length of the common normal ${}^i l_{i+1}$, α_i the rotation angle around the ${}^{i+1}x$ axis between the ${}^i z$ and the ${}^{i+1}z$ axes, d_i the distance between the common normal ${}^i l_{i+1}$ and \mathcal{O}_i , θ_i the rotation angle around the ${}^i z$ axis between the common normal ${}^i l_{i+1}$ and the ${}^i x$ axis. Then, the transformation matrix ${}^i T_{i+1}$ from Σ_{i+1} to Σ_i is given by

$${}^i T_{i+1} = \begin{pmatrix} \cos \theta_i & -\sin \theta_i \cos \alpha_i & \sin \theta_i \sin \alpha_i & a_i \cos \theta_i \\ \sin \theta_i & \cos \theta_i \cos \alpha_i & -\cos \theta_i \sin \alpha_i & a_i \sin \theta_i \\ 0 & \sin \alpha_i & \cos \alpha_i & d_i \\ 0 & 0 & 0 & 1 \end{pmatrix}. \quad (1)$$

In the coordinate transformation of myCobot in RViz, in addition to the transformation in (1), we add δ_i as the rotation angle around the ${}^{i+1}z$ axis between the ${}^i x$ and the ${}^{i+1}x$ axes. Thus, the transformation matrix A_i from Σ_{i+1} to Σ_i with respect to the coordinate transformation in RViz is given as

$$A_i = \begin{pmatrix} \cos \delta_i \cos \theta_i - \cos \alpha_i \sin \delta_i \sin \theta_i - \cos \alpha_i \cos \delta_i \sin \theta_i - \sin \delta_i \cos \theta_i & \cos \alpha_i \sin \delta_i \cos \theta_i + \cos \delta_i \sin \theta_i & \cos \alpha_i \cos \delta_i \cos \theta_i - \sin \delta_i \sin \theta_i & \sin \alpha_i \sin \theta_i & a_i \cos \theta_i \\ \sin \alpha_i \sin \delta_i & \sin \alpha_i \cos \delta_i & \sin \alpha_i \cos \delta_i & \sin \alpha_i \sin \theta_i & a_i \cos \theta_i \\ 0 & 0 & 0 & -\sin \alpha_i \cos \theta_i & a_i \sin \theta_i \\ 0 & 0 & 0 & \cos \alpha_i & d_i \\ 0 & 0 & 0 & 0 & 1 \end{pmatrix}, \quad (2)$$

where the joint parameters are given in Table 1.

Let A be the transformation matrix from the end-effector's coordinate system Σ_7 to the global coordinate system Σ_1 . Then, A is expressed as

$$A = A_1 A_2 A_3 A_4 A_5 A_6. \quad (3)$$

2.3 Description of the Orientation of the End-effector

Among the various methods to describe the orientation of the end-effector, this paper uses Roll-Pitch-Yaw angles [19]. Let $\mathbf{l}, \mathbf{m}, \mathbf{n}$ be the unit vectors of the

x, y, z -axis of the end-effector, respectively, as

$$\mathbf{l} = {}^t(l_1, l_2, l_3), \quad \mathbf{m} = {}^t(m_1, m_2, m_3), \quad \mathbf{n} = {}^t(n_1, n_2, n_3). \quad (4)$$

Then, the orientation of the end-effector is expressed as $(\mathbf{l} \ \mathbf{m} \ \mathbf{n})$. To express the orientation of the end-effector with the variables of 3-DOF, we use a series of the following rotations. First, rotate around the z -axis by γ (yaw angle), then rotate around the y -axis by β (pitch angle). Finally, rotate around the x -axis by α (roll angle) to represent any orientation in 3D space. Multiplying the rotation matrices of these rotations in order, we have a rotation matrix as

$$(\mathbf{l} \ \mathbf{m} \ \mathbf{n}) = \begin{pmatrix} \cos \beta \cos \gamma & \cos \beta \sin \gamma & -\sin \beta \\ \sin \alpha \sin \beta \cos \gamma - \cos \alpha \sin \gamma & \sin \alpha \sin \beta \sin \gamma + \cos \alpha \cos \gamma & \sin \alpha \cos \beta \\ \cos \alpha \sin \beta \cos \gamma + \sin \alpha \sin \gamma & \cos \alpha \sin \beta \sin \gamma - \sin \alpha \cos \gamma & \cos \alpha \cos \beta \end{pmatrix}. \quad (5)$$

2.4 Description of the Inverse Kinematic Problem of MyCobot

Let the orientation $\mathbf{l}, \mathbf{m}, \mathbf{n}$ of myCobot be given as in (4) and A be the transformation matrix in (3). Let $\mathbf{p} = {}^t(p_1, p_2, p_3)$ be the position of the end-effector w.r.t. Σ_1 . Since $\mathbf{l}, \mathbf{m}, \mathbf{n}$ are the unit vectors of the x, y, z -axis of Σ_7 , respectively, and \mathbf{p} is the position of the end-effector with respect to Σ_1 , we have A and A^{-1} as

$$A = \begin{pmatrix} l_1 & m_1 & n_1 & p_1 \\ l_2 & m_2 & n_2 & p_2 \\ l_3 & m_3 & n_3 & p_3 \\ 0 & 0 & 0 & 1 \end{pmatrix}, \quad A^{-1} = \begin{pmatrix} l_1 & l_2 & l_3 & -(l_1 p_1 + l_2 p_2 + l_3 p_3) \\ m_1 & m_2 & m_3 & -(m_1 p_1 + m_2 p_2 + m_3 p_3) \\ n_1 & n_2 & n_3 & -(n_1 p_1 + n_2 p_2 + n_3 p_3) \\ 0 & 0 & 0 & 1 \end{pmatrix}. \quad (6)$$

which establishes the inverse kinematic equation of myCobot. For given $\mathbf{l}, \mathbf{m}, \mathbf{n}$, and \mathbf{p} , the inverse kinematic problem is to find the joint angles $\theta_1, \dots, \theta_6$.

3 Solving the Inverse Kinematic Problem of MyCobot

In this section, we propose a solution to myCobot's inverse kinematics problem. First, we define the necessary notation.

- Vectors are represented in bold, such as \mathbf{P} or \mathbf{w} .
- A vector in the coordinate system Σ_i is represented as ${}^i\mathbf{P}$. If it is clear from the context that the vector is in Σ_1 , the superscript is unnecessary.
- A vector ${}^i\mathbf{P}$ is represented as ${}^j[{}^i\mathbf{P}]$ w.r.t. the coordinate system Σ_j .
- For a vector \mathbf{P} , the i th element is represented as $\mathbf{P}[i]$.

3.1 Conventional Algebraic Method and Pieper's Approach

To solve the inverse kinematics problem (6), substitute the components of the end-effector's orientation and position into the right-hand side and compare the corresponding elements of the matrices on both sides. Then, we obtain a system of 12 polynomial equations with respect to $\sin \theta_i$ and $\cos \theta_i$ for $i = 1, \dots, 6$. By appropriately selecting 6 of these equations and substituting $\sin \theta_i$ and $\cos \theta_i$ with $t_i = \tan \frac{\theta_i}{2}$, where $\sin \theta_i = \frac{2t_i}{1+t_i^2}$ and $\cos \theta_i = \frac{1-t_i^2}{1+t_i^2}$, we obtain six polynomial equations with six variables t_i . By eliminating one variable at a time, we derive a univariate polynomial equation from which each variable can be solved with backward substitution. However, according to Pieper [17], the degree of the resulting univariate equation exceeds 500000, making it difficult to solve the inverse kinematics problem of a 6-DOF manipulator using algebraic methods in general. Manocha and Canny [10] have proposed a method to solve the inverse kinematics problem of a general 6-DOF manipulator.

Generally, a 6-DOF manipulator cannot independently determine the orientation and position of the end-effector. Thus, it is difficult to solve the general inverse kinematics problem analytically. *However, if the manipulator includes a spherical joint with 3-dimensional rotation, the orientation and position of the end-effector can be determined independently.* Then, the inverse kinematics problem can be separated into a 3-dimensional problem for orientation and a 3-dimensional problem for position. In this case, the inverse kinematics problem will likely be solved analytically.

Pieper [17] has demonstrated that if the rotational axes of three consecutive rotational joints intersect at a single point, the motion of these three joints is kinematically equivalent to a spherical joint. He has proposed a solution to the inverse kinematics problem, focusing on this intersection point. Unfortunately, in myCobot, the rotational axes of consecutive joints that intersect at a single point are Joint 1 and Joint 2, Joint 4 and Joint 5, and Joint 5 and Joint 6, meaning there is no intersection point for the rotational axes of three joints, which means that Pieper's method cannot be directly applied. However, we have solved myCobot's inverse kinematics problem based on his approach. Specifically, we express the intersection point of the rotational axes of two joints by the position and the orientation of the end-effector, and then derive the rotation angles of the joints using this intersection point.

3.2 Deriving the Rotation Angle of the Joints

Let P be the intersection point of the rotational axes of Joints 4 and 5 as

$$\mathbf{P} = {}^t(x, y, z). \quad (7)$$

Note that \mathbf{P} is at the origin of Σ_5 . We express $\sin \theta_i$ and $\cos \theta_i$ in terms of x, y, z for $i = 1, \dots, 6$.

Remark 1. In solving the inverse kinematic problem, we use the transformation matrix A and its inverse A^{-1} in (6) and the orientation of the end-effector in (4).

Note that the orientation of the end-effector is not represented using the Roll-Pitch-Yaw angles but rather by the components l_i, m_i , and n_i for $i = 1, 2, 3$. Furthermore, since \mathbf{l} , \mathbf{m} , and \mathbf{n} are the unit vectors in the direction of each axis of Σ_7 , note that the following relationships hold.

$$\begin{aligned} l_2 m_3 - l_3 m_2 &= n_1, & l_3 m_1 - l_1 m_3 &= n_2, & l_1 m_2 - l_2 m_1 &= n_3, \\ l_1^2 + m_1^2 + n_1^2 &= 1, & l_2^2 + m_2^2 + n_2^2 &= 1, & l_3^2 + m_3^2 + n_3^2 &= 1, \\ l_1 l_2 + m_1 m_2 + n_1 n_2 &= 0, & l_2 l_3 + m_2 m_3 + n_2 n_3 &= 0, \\ l_3 l_1 + m_3 m_1 + n_3 n_1 &= 0. \end{aligned} \quad (8)$$

Now, for each $i = 1, \dots, 6$, determine $\sin \theta_i$ and $\cos \theta_i$ using the coordinates x, y, z of the intersection point \mathbf{P} .

Deriving $\sin \theta_6$ and $\cos \theta_6$ The position vector ${}^7\mathbf{P} = \overrightarrow{\mathcal{O}_7\mathbf{P}}$ is expressed in the following two ways. The intersection point \mathbf{P} is located at the origin of Σ_5 , so it can be expressed as

$${}^7\mathbf{P} = A_6^{-1} A_5^{-1} {}^t(0, 0, 0, 1) = {}^t(d_5 \sin \theta_6, d_5 \cos \theta_6, -d_6, 1). \quad (9)$$

On the other hand, since $\mathbf{P} = {}^t(x, y, z, 1)$, it can be expressed as

$${}^7\mathbf{P} = A^{-1} \begin{pmatrix} x \\ y \\ z \\ 1 \end{pmatrix} = \begin{pmatrix} l_1(-p_1 + x) + l_2(-p_2 + y) + l_3(-p_3 + z) \\ m_1(-p_1 + x) + m_2(-p_2 + y) + m_3(-p_3 + z) \\ n_1(-p_1 + x) + n_2(-p_2 + y) + n_3(-p_3 + z) \\ 1 \end{pmatrix}. \quad (10)$$

Since each element in the rightmost-hand-side of (9) and (10) is equal, we have

$$\begin{aligned} \sin \theta_6 &= \frac{l_1(-p_1 + x) + l_2(-p_2 + y) + l_3(-p_3 + z)}{d_5}, \\ \cos \theta_6 &= \frac{m_1(-p_1 + x) + m_2(-p_2 + y) + m_3(-p_3 + z)}{d_5}. \end{aligned} \quad (11)$$

Deriving $\sin \theta_5$ and $\cos \theta_5$ Let \mathbf{w} be the unit vector in the direction of the joint axis of Joint 4. Then, \mathbf{w}_4 and ${}^7[\mathbf{w}_4]$ are expressed as

$$\begin{aligned} \mathbf{w}_4 &= A_1 A_2 A_3 {}^t(0, 0, 1, 0) = {}^t(\sin \theta_1, -\cos \theta_1, 0, 0), \\ {}^7[\mathbf{w}_4] &= A_6^{-1} A_5^{-1} A_4^{-1} {}^t(0, 0, 1, 0) \\ &= {}^t(\cos \theta_5 \cos \theta_6, -\cos \theta_5 \sin \theta_6, -\sin \theta_5, 0). \end{aligned} \quad (12)$$

On the other hand, we also have

$$\mathbf{w}_4 = A \cdot {}^7[\mathbf{w}_4] = \begin{pmatrix} -n_1 \sin \theta_5 + \cos \theta_5 (l_1 \cos \theta_6 - m_1 \sin \theta_6) \\ -n_2 \sin \theta_5 + \cos \theta_5 (l_2 \cos \theta_6 - m_2 \sin \theta_6) \\ -n_3 \sin \theta_5 + \cos \theta_5 (l_3 \cos \theta_6 - m_3 \sin \theta_6) \\ 0 \end{pmatrix}. \quad (13)$$

Since each element of \mathbf{w}_4 in (12) and (13) is equal. By comparing the third element, we have

$$-n_3 \sin \theta_5 + \cos \theta_5 (l_3 \cos \theta_6 - m_3 \sin \theta_6) = 0. \quad (14)$$

By substituting $\sin \theta_6$ and $\cos \theta_6$ from (11) into (14) and simplifying using (8), we have

$$\begin{aligned} d_5 n_3 \sin \theta_5 + \cos \theta_5 (n_2(p_1 - x) - n_1(p_2 - y)) &= 0, \\ (\sin \theta_5)^2 + (\cos \theta_5)^2 &= 1. \end{aligned} \quad (15)$$

In the case $n_3 \neq 0$ or $n_2(p_1 - x) - n_1(p_2 - y) \neq 0$, by (15), $\sin \theta_5$ and $\cos \theta_5$ are expressed as

$$\begin{aligned} \sin \theta_5 &= \pm \frac{n_2(p_1 - x) - n_1(p_2 - y)}{\sqrt{d_5^2 n_3^2 + (n_2(p_1 - x) - n_1(p_2 - y))^2}}, \\ \cos \theta_5 &= \mp \frac{d_5 n_3}{\sqrt{d_5^2 n_3^2 + (n_2(p_1 - x) - n_1(p_2 - y))^2}}. \end{aligned} \quad (16)$$

In the case where $n_3 = 0$ and $n_2(p_1 - x) - n_1(p_2 - y) = 0$, it is described in Sect. 3.4.

Deriving $\sin \theta_1$ and $\cos \theta_1$ For $\sin \theta_1$ and $\cos \theta_1$, a comparison of the first and the second components of \mathbf{w}_4 in (12) and (13) shows that

$$\begin{aligned} \sin \theta_1 &= -n_1 \sin \theta_5 + \cos \theta_5 (l_1 \cos \theta_6 - m_1 \sin \theta_6), \\ \cos \theta_1 &= n_2 \sin \theta_5 - \cos \theta_5 (l_2 \cos \theta_6 - m_2 \sin \theta_6). \end{aligned} \quad (17)$$

By substituting $\sin \theta_6, \cos \theta_6, \sin \theta_5, \cos \theta_5$ from (11) and (16) and using (8), $\sin \theta_1$ and $\cos \theta_1$ are expressed as

$$\begin{aligned} \sin \theta_1 &= \pm \frac{-n_1 n_2 (p_1 - x) + (1 - n_2^2)(p_2 - y) - n_2 n_3 (p_3 - z)}{\sqrt{d_5^2 n_3^2 + (n_2(p_1 - x) - n_1(p_2 - y))^2}}, \\ \cos \theta_1 &= \pm \frac{(1 - n_1^2)(p_1 - x) - n_1 n_2 (p_2 - y) - n_1 n_3 (p_3 - z)}{\sqrt{d_5^2 n_3^2 + (n_2(p_1 - x) - n_1(p_2 - y))^2}}. \end{aligned} \quad (18)$$

Deriving $\sin \theta_3$ and $\cos \theta_3$ Let $\mathbf{P}_3 = \overrightarrow{\mathcal{O}_1 \mathbf{P}}$. Since \mathbf{P} is the origin of Σ_5 , \mathbf{P}_3 satisfies $\mathbf{P}_3 = \overrightarrow{\mathcal{O}_1 \mathcal{O}_5}$ as

$$\begin{aligned} \mathbf{P}_3 &= A_1 A_2 A_3 A_4 {}^t(0, 0, 0, 1) \\ &= \begin{pmatrix} d_4 \sin \theta_1 - a_2 \cos \theta_1 \sin \theta_2 - a_3 \cos \theta_1 (\sin \theta_2 \cos \theta_3 + \cos \theta_2 \sin \theta_3) \\ -d_4 \cos \theta_1 - a_2 \sin \theta_1 \sin \theta_2 - a_3 \sin \theta_1 (\sin \theta_2 \cos \theta_3 + \cos \theta_2 \sin \theta_3) \\ d_1 + a_2 \cos \theta_2 + a_3 (\cos \theta_2 \cos \theta_3 - \sin \theta_2 \sin \theta_3) \\ 1 \end{pmatrix}. \end{aligned} \quad (19)$$

On the other hand, since the coordinate of \mathbf{P} is ${}^t(x, y, z)$, \mathbf{P}_3 is expressed as

$$\mathbf{P}_3 = {}^t(x, y, z, 1). \quad (20)$$

Let $Q = \mathbf{P}_3[1]^2 + \mathbf{P}_3[2]^2 + (\mathbf{P}_3[3] - d_1)^2$. By calculating Q using the components in (19) and (20), we have

$$a_2^2 + a_3^2 + d_4^2 + 2a_2a_3 \cos \theta_3 = x^2 + y^2 + (z - d_1)^2. \quad (21)$$

Thus, $\sin \theta_3$ and $\cos \theta_3$ are expressed as

$$\sin \theta_3 = \pm \sqrt{1 - (\cos \theta_3)^2}, \quad \cos \theta_3 = \frac{x^2 + y^2 + (z - d_1)^2 - a_2^2 - a_3^2 - d_4^2}{2a_2a_3}. \quad (22)$$

Deriving $\sin \theta_2$ and $\cos \theta_2$ By comparing the third component of \mathbf{P}_3 in (19) and (20), we have

$$\begin{aligned} d_1 - a_2 \cos \theta_2 - a_3(\cos \theta_2 \cos \theta_3 - \sin \theta_2 \sin \theta_3) &= z, \\ (\sin \theta_2)^2 + (\cos \theta_2)^2 &= 1. \end{aligned} \quad (23)$$

Thus, $\sin \theta_2$ and $\cos \theta_2$ can be obtained by substituting the expressions for $\sin \theta_3$ and $\cos \theta_3$ from (22) into (23).

Deriving $\sin \theta_4$ and $\cos \theta_4$ Let \mathbf{w}_5 be the unit vector in the direction of the joint axis of Joint 5. Then we have ${}^5[\mathbf{w}_5] = {}^t(0, 0, 1, 0)$. Thus, \mathbf{w}_5 and ${}^7[\mathbf{w}_5]$ are expressed as

$$\begin{aligned} \mathbf{w}_5 &= A_1 A_2 A_3 A_4 \begin{pmatrix} 0 \\ 0 \\ 1 \\ 0 \end{pmatrix} = \begin{pmatrix} -\cos \theta_1 \sin(\theta_2 + \theta_3 + \theta_4) \\ -\sin \theta_1 \sin(\theta_2 + \theta_3 + \theta_4) \\ \cos(\theta_2 + \theta_3 + \theta_4) \\ 0 \end{pmatrix}, \\ {}^7[\mathbf{w}_5] &= A_6^{-1} A_5^{-1} {}^t(0, 0, 1, 0) = {}^t(-\sin \theta_6, -\cos \theta_6, 0, 0). \end{aligned} \quad (24)$$

On the other hand, we also have

$$\mathbf{w}_5 = A \cdot {}^7[\mathbf{w}_5] = \begin{pmatrix} -m_1 \cos \theta_6 - l_1 \sin \theta_6 \\ -m_2 \cos \theta_6 - l_2 \sin \theta_6 \\ -m_3 \cos \theta_6 - l_3 \sin \theta_6 \\ 0 \end{pmatrix}. \quad (25)$$

Since each element in the rightmost-hand-side of \mathbf{w}_5 in (24) and (25) is equal, by comparing the third element, we have

$$\begin{aligned} \cos(\theta_2 + \theta_3 + \theta_4) &= (\cos \theta_2 \cos \theta_3 - \sin \theta_2 \sin \theta_3) \cos \theta_4 \\ &\quad - (\sin \theta_2 \cos \theta_3 + \cos \theta_2 \sin \theta_3) \sin \theta_4 \\ &= -m_3 \cos \theta_6 - l_3 \sin \theta_6, \\ (\cos \theta_4)^2 + (\sin \theta_4)^2 &= 1. \end{aligned} \quad (26)$$

Furthermore, $\sin \theta_4$ and $\cos \theta_4$ can be obtained by substituting the expressions for $\sin \theta_i$ and $\cos \theta_i$ for $i = 1$ (in (18)), 2 (in (23)), 3 (in (22)), and 6 (in (11)) into (26).

3.3 Deriving the Intersection Point

We derive x, y , and z of the intersection point \mathbf{P} in (7). First, by comparing the third component of the vector ${}^7\mathbf{P}$ from (9) and (10), we have

$$n_1(p_1 - x) + n_2(p_1 - y) + n_3(p_3 - z) = d_6. \quad (27)$$

Next, comparing the third component of the vector ${}^7\mathbf{P}$ from (9) and (10), we see that

$$\begin{aligned} \|{}^7\mathbf{P}\|^2 &= d_5^2 + d_6^2, \\ \|{}^7\mathbf{P}\|^2 &= (l_1(-p_1 + x) + l_2(-p_2 + y) + l_3(-p_3 + z))^2 \\ &\quad + (m_1(-p_1 + x) + m_2(-p_2 + y) + m_3(-p_3 + z))^2 \\ &\quad + (n_1(-p_1 + x) + n_2(-p_2 + y) + n_3(-p_3 + z))^2 \\ &= (l_1^2 + m_1^2 + n_1^2)(p_1 - x)^2 + (l_2^2 + m_2^2 + n_2^2)(p_2 - y)^2 \\ &\quad + (l_3^2 + m_3^2 + n_3^2)(p_3 - z)^2 \\ &\quad + 2(l_1l_2 + m_1m_2 + n_1n_2)(p_1 - x)(p_2 - y) \\ &\quad + 2(l_2l_3 + m_2m_3 + n_2n_3)(p_2 - y)(p_3 - z) \\ &\quad + 2(l_3l_1 + m_3m_1 + n_3n_1)(p_3 - z)(p_1 - x) \\ &= (p_1 - x)^2 + (p_2 - y)^2 + (p_3 - z)^2. \end{aligned} \quad (28)$$

Thus, we have

$$(p_1 - x)^2 + (p_2 - y)^2 + (p_3 - z)^2 = d_5^2 + d_6^2. \quad (29)$$

Thirdly, let ${}^5\mathcal{O}_1 = \overrightarrow{P\mathcal{O}_1}$. Considering it as a position vector, using the transformation matrices $A_1^{-1}, A_2^{-1}, A_3^{-1}, A_4^{-1}$, it can be expressed as

$$\begin{aligned} {}^5\mathcal{O}_1 &= A_4^{-1}A_3^{-1}A_2^{-1}A_1^{-1} \cdot {}^t(0, 0, 0, 1) \\ &= \begin{pmatrix} -d_4 \\ -a_3 \sin \theta_4 - a_2 \sin(\theta_3 + \theta_4) - d_1 \sin(\theta_2 + \theta_3 + \theta_4) \\ -a_3 \cos \theta_4 - a_2 \cos(\theta_3 + \theta_4) - d_1 \cos(\theta_2 + \theta_3 + \theta_4) \\ 1 \end{pmatrix}. \end{aligned} \quad (30)$$

Additionally, the vector $\overrightarrow{P\mathcal{O}_1}$ and the vector $\overrightarrow{\mathcal{O}_1P}$ are vectors in opposite directions. Therefore, in the coordinate system Σ_1 , the direction vector ${}^1[\overrightarrow{P\mathcal{O}_1}] = {}^1[{}^5\mathcal{O}_1] = (-x, -y, -z, 0)^T$ holds. Consequently, ${}^5\mathcal{O}_1$ can also be expressed as

$$\begin{aligned} {}^5\mathcal{O}_1 &= A_4^{-1}A_3^{-1}A_2^{-1}A_1^{-1} \cdot {}^1[{}^5\mathcal{O}_1] = {}^t(\mathcal{O}_{1,1}, \mathcal{O}_{1,2}, \mathcal{O}_{1,3}, 0), \\ \mathcal{O}_{1,1} &= y \cos \theta_1 - x \sin \theta_1, \\ \mathcal{O}_{1,2} &= \frac{1}{2}(-x(\cos \theta_{1-2-3-4} + \cos \theta_{1+2+3+4}) \\ &\quad - y(\sin \theta_{1-2-3-4} + \sin \theta_{1+2+3+4}) - 2z \sin \theta_{2+3+4}), \\ \mathcal{O}_{1,3} &= \frac{1}{2}(-x(\sin \theta_{1-2-3-4} - \sin \theta_{1+2+3+4}) \\ &\quad + y(\cos \theta_{1-2-3-4} - \cos \theta_{1+2+3+4}) - 2z \cos \theta_{2+3+4}). \end{aligned} \quad (31)$$

where $\theta_{1-2-3-4} = \theta_1 - \theta_2 - \theta_3 - \theta_4$, $\theta_{1+2+3+4} = \theta_1 + \theta_2 + \theta_3 + \theta_4$, $\theta_{2+3+4} = \theta_2 + \theta_3 + \theta_4$.

The first, second, and third components of ${}^5\mathbf{O}_1$ in (30) and (31) are equal, respectively. The comparison of the first component shows that

$$y \cos \theta_1 - x \sin \theta_1 = -d_4. \quad (32)$$

By substituting (18) into (32) and simplifying, the following holds.

$$\begin{aligned} \pm d_4 = & y \frac{(1 - n_1^2)(p_1 - x) - n_1 n_2(p_2 - y) - n_1 n_3(p_3 - z)}{\sqrt{d_5^2 n_3^2 + (n_2(p_1 - x) - n_1(p_2 - y))^2}} \\ & - x \frac{-n_1 n_2(p_1 - x) + (1 - n_2^2)(p_2 - y) - n_2 n_3(p_3 - z)}{\sqrt{d_5^2 n_3^2 + (n_2(p_1 - x) - n_1(p_2 - y))^2}}, \end{aligned}$$

thus we have

$$\begin{aligned} & d_4^2(d_5^2 n_3^2 + (n_2(p_1 - x) - n_1(p_2 - y))^2) \\ = & ((n_1 n_2 x + (1 - n_1^2)y)(p_1 - x) - (n_1 n_2 y + (1 - n_2^2)x)(p_2 - y) \\ & - n_3(n_1 y - n_2 x)(p_3 - z))^2. \end{aligned} \quad (33)$$

Therefore, the following system of parametric algebraic equations for x, y , and z is derived from equations (27), (29) and (33), as

$$\begin{aligned} & n_1(p_1 - x) + n_2(p_2 - y) + n_3(p_3 - z) = d_6, \\ & (p_1 - x)^2 + (p_2 - y)^2 + (p_3 - z)^2 = d_5^2 + d_6^2, \\ & ((n_1 n_2 x + (1 - n_1^2)y)(p_1 - x) \\ & - (n_1 n_2 y + (1 - n_2^2)x)(p_2 - y) - n_3(n_1 y - n_2 x)(p_3 - z))^2 \\ & = d_4^2(d_5^2 n_3^2 + (n_2(p_1 - x) - n_1(p_2 - y))^2), \end{aligned} \quad (34)$$

where parameters are n_1, n_2 , and n_3 (direction of the end-effector's z -axis), p_1, p_2 , and p_3 (position of the end-effector). Note that d_4, d_5 , and d_6 are the lengths of the links in the DH parameter (see Table 1). When actually solving (34), the lengths of the links are assigned to d_4, d_5 , and d_6 in terms of rational numbers.

When the orientation and position of the end-effector are given, by solving (34), the coordinates x, y, z of the intersection point \mathbf{P} can be determined. Then, $\sin \theta_i, \cos \theta_i$ ($i = 1, \dots, 6$) can be obtained using the method from above, allowing θ_i to be determined.

To solve (34), one can compute the Gröbner basis after substituting the orientation and position of the end-effector. However, the computation of the Gröbner basis each time after the substitution is time-consuming. Therefore, by following the approach of our previous research [16, 26], computing the CGS of the ideal generated by the polynomials in (34), the corresponding Gröbner basis can be quickly obtained once the orientation and position of the end-effector are given, significantly reducing the time required.

Remark 2. In (34), some equations are squared on both sides to eliminate complex signs and radicals, making it easier to compute the CGS. Then, the solution x, y, z of the intersection point \mathbf{P} and the solutions to the inverse kinematics problem may include values that differ from the original solutions. Thus, after solving the inverse kinematics problem, it is necessary to solve the forward kinematic problem to verify the results.

3.4 Deriving and Solving the Inverse Kinematics Problem for Special Orientations

The above method cannot be used when the end-effector's orientation is horizontal to the ground, i.e., when $n_3 = 0$. In the case $n_3 = 0$, problems arise in (15) and (34). We discuss these issues and their solutions.

In the Case $n_3 = 0$ and $n_2(p_1 - x) - n_1(p_2 - y) = 0$ When certain x, y satisfy $n_3 = 0$ and $n_2(p_1 - x) - n_1(p_2 - y) = 0$, the equation $d_5 n_3 \sin \theta_5 + \cos \theta_5 (n_2(p_1 - x) - n_1(p_2 - y))$ in (15) becomes identically zero. Consequently, $\sin \theta_5$ and $\cos \theta_5$ cannot be determined, and $\sin \theta_1$, $\cos \theta_1$ derived from $\sin \theta_5$, $\cos \theta_5$, as well as (33), cannot be obtained. Therefore, a new method for determining $\sin \theta_1$, $\cos \theta_1$, $\sin \theta_5$, $\cos \theta_5$, and the coordinates x, y, z of the intersection point P is established.

We first calculate x, y , and z . From the assumptions of this case, we have

$$n_2(p_1 - x) - n_1(p_2 - y) = 0. \quad (35)$$

Furthermore, (27) and (29) hold regardless of the current assumptions. Therefore, the values of x, y, z that vanish $d_5 n_3 \sin \theta_5 + \cos \theta_5 (n_2(p_1 - x) - n_1(p_2 - y))$ in (15) can be determined from the following system of parametric equations:

$$\begin{aligned} n_1(p_1 - x) + n_2(p_2 - y) &= d_6, \\ (p_1 - x)^2 + (p_2 - y)^2 + (p_3 - z)^2 &= d_5^2 + d_6^2, \\ n_2(p_1 - x) - n_1(p_2 - y) &= 0, \end{aligned} \quad (36)$$

where parameters are n_1 and n_2 (direction of the end-effector's z -axis), p_1, p_2 , and p_3 (position of the end-effector). Note that d_5, d_6 are the lengths of the links in the DH parameter and, in actual calculations, real numbers are substituted.

Next, for $\sin \theta_1$ and $\cos \theta_1$, by comparing the first component of \mathbf{P}_3 from (19) and (20), we have

$$\begin{aligned} d_4 \sin \theta_1 - a_2 \cos \theta_1 \sin \theta_2 - a_3 \cos \theta_1 (\sin \theta_2 \cos \theta_3 + \cos \theta_2 \sin \theta_3) &= x, \\ (\sin \theta_1)^2 + (\cos \theta_1)^2 &= 1. \end{aligned} \quad (37)$$

Once x, y , and z are determined from (36), $\sin \theta_2$, $\cos \theta_2$, $\sin \theta_3$, and $\cos \theta_3$ can be obtained. By substituting the obtained results into (37), $\sin \theta_1$ and $\cos \theta_1$ can be determined.

For $\sin \theta_5$ and $\cos \theta_5$, by comparing the first component of \mathbf{w}_4 from (12) and (13), we have

$$\begin{aligned} -n_1 \sin \theta_5 + \cos \theta_5 (l_1 \cos \theta_6 - m_1 \sin \theta_6) &= \sin \theta_1, \\ -n_2 \sin \theta_5 + \cos \theta_5 (l_2 \cos \theta_6 - m_2 \sin \theta_6) &= -\cos \theta_1. \end{aligned} \quad (38)$$

$\sin \theta_6$ and $\cos \theta_6$ can be obtained in the same way as in Sect. 3.2. $\sin \theta_1$ and $\cos \theta_1$ can be determined from (37). By substituting these into (38), $\sin \theta_5$ and $\cos \theta_5$ can be obtained.

In the Case $n_3 = 0$ and $n_2(p_1 - x) - n_1(p_2 - y) \neq 0$ Assume that $n_3 = 0$ and $n_2(p_1 - x) - n_1(p_2 - y) \neq 0$. By putting $n_3 = 0$ into (27), we have $n_1(p_1 - x) + n_2(p_2 - y) = d_6$, which derives $n_1x + n_2y = n_1p_1 + n_2p_2 - d_6$. Next, by substituting $n_3 = 0$ into (33), we have

$$(n_2(p_1 - x) - n_1(p_2 - y))^2 (n_1x + n_2y)^2 = d_4^2 (n_2(p_1 - x) - n_1(p_2 - y))^2,$$

which derives $(n_1x + n_2y)^2 = d_4^2$, or $n_1x + n_2y = \pm d_4$. We see that, for (34) to have a solution, $n_1p_1 + n_2p_2 - d_6 = \pm d_4$ must hold. Additionally, even if $n_1p_1 + n_2p_2 - d_6 = \pm d_4$ is satisfied, there are only two equations for three variables, so the solution may not be unique. Thus, it is necessary to find one more equation for x, y , and z .

By substituting $n_3 = 0$ into (18), $\sin \theta_1$ and $\cos \theta_1$ can be expressed as

$$\sin \theta_1 = \pm n_1, \quad \cos \theta_1 = \mp n_2. \quad (39)$$

Furthermore, by substituting (39) into the components of \mathbf{P}_3 in (19), and comparing each component with those in (20), we have

$$\begin{aligned} \pm d_4 n_1 \pm a_2 n_2 \sin \theta_2 \pm a_3 n_2 (\sin \theta_2 \cos \theta_3 + \cos \theta_2 \sin \theta_3) &= x, \\ \pm d_4 n_2 \mp a_2 n_1 \sin \theta_2 \mp a_3 n_1 (\sin \theta_2 \cos \theta_3 + \cos \theta_2 \sin \theta_3) &= y, \\ d_1 + a_2 \cos \theta_2 + a_3 (\cos \theta_2 \cos \theta_3 - \sin \theta_2 \sin \theta_3) &= z, \\ (\sin \theta_2)^2 + (\cos \theta_2)^2 &= 1, \quad (\sin \theta_3)^2 + (\cos \theta_3)^2 = 1. \end{aligned} \quad (40)$$

In (40), solving equations 1, 3, 4, and 5 for $\sin \theta_2, \cos \theta_2, \sin \theta_3$, and $\cos \theta_3$ yields two sets of solutions. In this case, $\cos \theta_3$ is expressed as

$$\cos \theta_3 = \frac{d_4^2 n_1^2 - a_2^2 n_2^2 - a_3^2 n_2^2 + d_1^2 n_2^2 \mp 2d_4 n_1 x + x^2 - 2d_1 n_2^2 z + n_2^2 z^2}{2a_2 a_3 n_2^2},$$

for both sets. By substituting the above $\cos \theta_3$ into $\cos \theta_3$ in (21), the following holds. In the case $n_2 \neq 0$, we have

$$\frac{d_4^2 \mp 2d_4 n_1 x + n_1^2 x^2 - n_2^2 y^2}{n_2^2} = 0,$$

which derives

$$(d_4^2 + n_1^2 x^2 - n_2^2 y^2)^2 - 4d_4^2 n_1^2 x^2 = 0. \quad (41)$$

In the case $n_2 = 0$, performing the same calculations as above for equations 1, 2, 4, and 5 in (40), we have

$$(d_4^2 - n_1^2 x^2 + n_2^2 y^2)^2 - 4d_4^2 n_2^2 y^2 = 0. \quad (42)$$

Thus, x, y, z can be obtained by solving (34) along with either (41) or (42).

3.5 An algorithm

Based on the above results, the algorithm for solving the inverse kinematics problem of myCobot is shown in Algorithm 1 (Note that Algorithm 1 reflects the flow of calculations from Sect. 3.2 to 3.4). In Algorithm 1, the order in which each θ_i is determined is partially unordered. However, note that we must calculate θ_3, θ_2 , and θ_4 in order in Sect. 3.2, and θ_3, θ_2 , and θ_1 in order in Sect. 3.4. Furthermore, if multiple solutions are obtained for each θ_i , it is necessary to determine the set $(\theta_1, \dots, \theta_6)$ for each case.

4 Implementation and Experiments

In this section, we present an optimization of Algorithm 1, an implementation and the experimental results of the proposed algorithm.

4.1 Efficient Calculation of $\sin \theta_i$ and $\cos \theta_i$ with Gröbner Basis Computation

Algorithm 1 performs the calculation of $\cos \theta_i$ and $\sin \theta_i$ ($i = 1, \dots, 6$), according to the calculation described in Sect. 3. For $i = 1, \dots, 6$, let $c_i = \cos \theta_i$ and $s_i = \sin \theta_i$. In the generic case, the equations with respect to s_i and c_i are derived as a system of 12 polynomial equations $f_1 = \dots = f_{12} = 0$, derived from (11), (15), (17), (21) and (23), and (26). Then, for solving $f_1 = \dots = f_{12} = 0$, we calculate the Gröbner basis G of the ideal $\langle f_1, \dots, f_{12} \rangle$ in $\mathbb{R}(l_1, l_2, l_3, m_1, m_2, m_3, n_1, n_2, n_3, p_1, p_2, p_3, x, y, z)$ $[c_1, s_1, c_2, s_2, c_3, s_3, c_4, s_4, c_5, s_5, c_6, s_6]$ with the lexicographic order $s_4 > c_4 > s_2 > c_2 > s_3 > c_3 > s_1 > c_1 > s_5 > c_5 > s_6 > c_6$.

In the following experimental results, the use of G significantly reduced the computing time, and it also improved the computation accuracy (see the experimental results in Sect. 4.4).

Note that, unless otherwise noted, all the following calculation results are obtained using Algorithm 1 together with the pre-computed Gröbner basis G .

4.2 Implementation

We have implemented Algorithm 1 on the computer algebra system Risa/Asir [14]. The CGS calculations were performed using the implementation on Risa/Asir by Nabeshima [11], which implements the algorithm by Kapur et al. [7]. The

Algorithm 1 Solving the inverse kinematic problem in myCobot

Input: The end-effector's position $\mathbf{p} = (p_1, p_2, p_3)$ and orientation (α, β, γ) ;
Output: A set K' of tuples of joint angles $(\theta_1, \dots, \theta_6)$;

- 1: Calculate CGS of (34) and (36);
- 2: Calculate l_i, m_i, n_i ($i = 1, 2, 3$) by substituting α, β, γ into (5);
- 3: $K \leftarrow \emptyset$; $K' \leftarrow \emptyset$;
- 4: **if** $n_3 = 0$ **then**
- 5: **if** $n_2(p_1 - x) - n_1(p_2 - y) = 0$ **then**
- 6: Choose an appropriate segment from the CGS of (36);
- 7: **else**
- 8: Choose an appropriate segment from the CGS of (34) along with (42) (for $n_2 = 0$) or (41) (for $n_2 \neq 0$);
- 9: **end if**
- 10: Substitute l_i, m_i, n_i, p_i ($i = 1, 2, 3$) in the CGS with the calculated values;
- 11: Calculate the intersection point (x, y, z) from the selected Gröbner basis;
- 12: Calculate $\theta_6, \theta_3, \theta_2, \theta_1, \theta_4, \theta_5$ sequentially from (11), (22), (23), (37), (26) and (38), respectively;
- 13: **else**
- 14: Choose an appropriate segment from the CGS of (34);
- 15: Substitute l_i, m_i, n_i, p_i ($i = 1, 2, 3$) in the CGS with the calculated values;
- 16: Calculate the intersection point (x, y, z) from the selected Gröbner basis;
- 17: Calculate $\theta_6, \theta_5, \theta_1, \theta_3, \theta_2, \theta_4$ sequentially from (11), (16), (18), (22), (23) and (26), respectively;
- 18: **end if**
- 19: $K \leftarrow K \cup \{(\theta_1, \theta_2, \theta_3, \theta_4, \theta_5, \theta_6)\}$;
- 20: **for each** $(\theta_1, \theta_2, \theta_3, \theta_4, \theta_5, \theta_6) \in K$ **do**
- 21: Substitute $(\theta_1, \theta_2, \theta_3, \theta_4, \theta_5, \theta_6)$ into the transformation matrix A of (3);
- 22: **if** $A = (\mathbf{l}, \mathbf{m}, \mathbf{n}, \mathbf{p})$ **then**
- 23: $K' \leftarrow K' \cup \{(\theta_1, \theta_2, \theta_3, \theta_4, \theta_5, \theta_6)\}$;
- 24: **end if**
- 25: **end for**
- 26: **return** K' .

functionality for computing numerical roots of univariate polynomial equations utilizes the capabilities of the computer algebra system PARI/GP 2.13.1 [22], which is invoked as a built-in function from Risa/Asir.

The computing environment is as follows: Intel Xeon Silver 4210 3.2 GHz, RAM 256 GB, Linux Kernel 5.4.0, Risa/Asir Version 20230315.

Remark 3. As we have mentioned in Remark 2, after solving the inverse kinematics problem, it is necessary to solve the forward kinematic problem to verify the results. While this procedure is included in line 22 of Algorithm 1, in our implementation, for efficiency, only the position of the end-effector \mathbf{p} is inspected.

4.3 Calculating the CGS

In this section, we show the calculation results of the CGS for the parametric systems of equations obtained in Sect. 3. We have calculated the CGS for the

Table 2. Computing time of CGS

Case	Time [s]	# Segments
1	> 2 Months	> 1
1 (the 1st segment)	2.58713	1
2	0.021623	9
3	0.001202	2
4	11.2487	11
5	10.0062	11

following cases of parametric systems of equations after substituting the DH parameters in Table 1: Case 1: (34); Case 2: substituting $n_1 = 0, n_2 = 0, n_3 = \pm 1$ in (34); Case 3: (36); Case 4: (34) along with (41); and Case 5: (34) along with (42).

Table 2 shows the computing time (in seconds) and the number of segments¹ of the CGS obtained. Although the calculation for (34) continued for about two months, a complete CGS was not obtained. However, the first segment and its corresponding Gröber basis was obtained in approximately 2.59 seconds, suggesting that the calculation of the other segments is time-consuming.

In our implementation of Algorithm 1, since only one segment of the CGS has been calculated, we assume that the position and orientation of the end effector in the input belong to the only calculated segment, and substitute them into the coefficients of the Gröbner basis to calculate the intersection point.

4.4 Accuracy of the Inverse Kinematic Solution

We first conducted an accuracy assessment of the inverse kinematic solution by evaluating how frequently solutions to the inverse kinematics problem were obtained by Algorithm 1, as well as evaluating the accuracy of those solutions. The accuracy assessment was conducted using the following procedure:

1. Randomly assign the set of $\theta_1, \dots, \theta_6$ within the feasible region of myCobot.
2. Substitute the $\theta_1, \dots, \theta_6$ obtained in Step 1 into A in (3) to determine the position and the orientation of the end-effector (solving the forward kinematics problem).
3. Apply Algorithm 1 to the position and the orientation of the end-effector obtained in Step 2 (solving the inverse kinematics problem).
4. Evaluate the number of times the solutions $\theta_i = (\theta_{i,1}, \dots, \theta_{i,6})$ obtained in Step 3 match the θ_i given in Step 1, as well as the average number of different solutions obtained.

Tables 3 and 4 show the results. For each test, 1000 samples of joint angles within the feasible region were randomly assigned, totaling 10000 samples. In the table, each column shows the following: “Avg. Time” shows the average time it

¹ Due to the lack of space, we refer to references (e.g., [21]) for segments and other key concepts of the CGS.

Table 3. Accuracy of the inverse kinematic solution *without* pre-computation of the Gröbner basis (see Sect. 4.4)

Test	Avg. Time [s]	# Success	# Diff. Soln.	Avg. # Soln.
1	0.502	998	5	6.139
2	0.535	994	5	6.114
3	0.504	993	2	6.183
4	0.497	999	2	6.035
5	0.474	996	2	6.140
6	0.552	998	2	6.052
7	0.490	997	3	6.114
8	0.492	998	4	6.019
9	0.479	996	8	5.966
10	0.508	995	4	6.032
Avg.	0.503	996.4	3.7	6.0794

Table 4. Accuracy of the inverse kinematic solution *with* pre-computation of the Gröbner basis (see Sect. 4.4)

Test	Avg. Time [s]	# Success	# Diff. Soln.	Avg. # Soln.
1	0.112	999	2	6.056
2	0.097	993	0	6.122
3	0.097	999	2	6.038
4	0.097	995	1	6.062
5	0.097	999	2	5.974
6	0.097	997	4	5.944
7	0.097	997	0	6.112
8	0.097	998	3	6.126
9	0.097	998	2	6.112
10	0.097	997	2	6.086
Avg.	0.099	997.2	1.8	6.0632

takes to solve the inverse kinematics problem in seconds², “# Success” shows the number of cases in which the given joint angles were obtained³, “# Diff. Soln.” shows the number of cases in which solutions are different from the given one were obtained, and “Avg. # Soln.” the average number of solutions obtained. The bottom row shows the average of each column.

In the experiments shown in Table 3, the pre-computation of the Gröbner basis described in Sect. 4.1 was not performed, whereas in the experiments shown in Table 4, this pre-computation was carried out. From both tables, we see that the pre-computation of the Gröbner basis reduces the computation time for

² Note that the computing time was rounded to the nearest millisecond.

³ The criterion for whether the inverse kinematic problem was successfully solved is an absolute error of less than 0.1 [mm] between the position of the end-effector obtained from the solution of the inverse kinematics problem and the position of the given end-effector. This is a reasonable criterion since the repeatability accuracy of myCobot is ± 0.5 [mm].

Table 5. Results of the inverse kinematics computation with randomly given position and orientation

Test	1	2	3	4	5	6	7	8	9	10	Avg.
# Success	393	371	374	355	336	386	360	393	355	406	372.9

solving the inverse kinematics problems to approximately one-fourth to one-fifth of the original time. Furthermore, throughout the experiments, the success rate of solving the inverse kinematics problems has improved, and the number of cases in which the obtained solutions differ from the given original joint configurations has decreased.

In the following, we present our observations based on the results shown in Table 4. The table shows that Algorithm 1 was able to calculate approximately 99.7 % of solutions to the inverse kinematic problems⁴. However, approximately 0.1 % of those solutions differed from the initially given solutions. (Note that, before optimization, the percentage of solutions that differed from the initially given solution was about 0.3 %.) This is likely due to errors arising from the numerical computation of trigonometric values in Risa/Asir, and the propagation of the errors during the backward substitution of x, y, z , and each θ_i .

We also see that the number of different solutions for each inverse kinematics problem averaged about 6 per sample. However, as mentioned earlier, there are cases where the solutions that should have been obtained were not, so this average value is only for reference.

In the experiment, the initial configuration of each joint $\theta_1, \dots, \theta_6$ is randomly assigned in Step 1. This is to guarantee the set of feasible positions and orientations for the end-effector. As we have mentioned above, in myCobot, it may not be possible to independently determine the position and the orientation of the end-effector since myCobot does not have three consecutive joints with intersecting rotational axes. To verify this, we conducted another experiment by randomly assigning the position and the orientation of the end-effector and applying Algorithm 1 to solve the inverse kinematics problem. Table 5 shows the results of the experiment. For each test, 1000 samples of the position and the orientation were randomly assigned, totaling 10000 samples. In the table, the column “# Success” shows the same value as Table 4. The result shows that only about 37.3 % of solutions can be obtained when the position and orientation of the end-effector are randomly assigned. This result suggests that there may be areas that cannot be reached by the end-effector in a particular orientation, even within the operating range of the link, due to the structure of the manipulator or other reasons.

⁴ For the remaining approximately 0.4% of the inverse kinematic problems, the position of the end-effector was not successfully obtained. The cause may be related to numerical instability in solving the system of polynomial equations, but a detailed investigation of the cause is a future issue.

4.5 Accuracy of the Forward Kinematic Solution

Next, we conducted an accuracy assessment of the forward kinematic solution by evaluating the discrepancy between the desired position and orientation of the end-effector for the inverse kinematics problem, and the position and orientation obtained from Algorithm 1 by the following procedure.

1. Randomly assign the set of $\theta_1, \dots, \theta_6$ within the feasible region of myCobot.
2. Substitute the $\theta_1, \dots, \theta_6$ obtained in Step 1 into A in (3) to determine the position and orientation of the end-effector (solving the forward kinematics problem).
3. Apply Algorithm 1 to the position and the orientation of the end-effector obtained in Step 2 (solving the inverse kinematics problem).
4. Substitute the solution θ_i obtained in Step 3 into A in (3) to obtain the position and the orientation of the end-effector.
5. Evaluate the errors of the position and orientation obtained in Step 4 from those obtained in Step 2.

As the function used for error evaluation (error evaluation function), we employ the error rate (relative error) ε , defined as $|(x - x')/x|$, where x is the theoretical value and x' is the measured value.

Let E'_i be the error evaluation function for one of the solutions to the inverse kinematics problem obtained by Algorithm 1. E'_i is obtained from the average error rate of six input values: three related to orientation (α, β, γ) and three related to position (p_1, p_2, p_3). Therefore, if the error rates for each input value are $\varepsilon_\alpha, \varepsilon_\beta, \varepsilon_\gamma, \varepsilon_{p_1}, \varepsilon_{p_2}, \varepsilon_{p_3}$, E'_i is defined as $E'_i = (\varepsilon_\alpha + \varepsilon_\beta + \varepsilon_\gamma + \varepsilon_{p_1} + \varepsilon_{p_2} + \varepsilon_{p_3})/6$. Table 4 shows that there is an average of about six solutions to the inverse kinematics problem per sample. Therefore, for the error evaluation functions E'_i calculated for each solution, the final error evaluation function E corresponding to a sample point is defined as the average value of E'_i ($i = 1, \dots, 6$), expressed as

$$E = \frac{1}{\#A} \sum_{i \in \{1, \dots, \#A\}} E'_i, \quad (43)$$

where A represents the set of solutions to the inverse kinematics problem obtained from Algorithm 1, and $\#A$ denotes the number of elements in A .

Figure 3 shows the results of the error evaluation. Note that the randomly generated samples here are the same as those used in Sect. 4.4. In the figure, the samples for which solutions to the inverse kinematics problem were obtained are shown in bright color, and the samples where the initially given $\theta_1, \dots, \theta_6$ did not match the output of Algorithm 1 are shown in dark color. From Figure 3, we see that approximately 95 % of the results have an error evaluation function E of less than 10^{-6} . Considering that the theoretical range of the end-effector's position (p_1, p_2, p_3) is approximately -200 [mm] to 400 [mm], the positional error is about 10^{-4} [mm]. Since the reproducibility of myCobot is ± 0.5 [mm], we see that the output of Algorithm 1 has sufficient accuracy. On the other hand, for the samples where the initially given $\theta_1, \dots, \theta_6$ did not match the

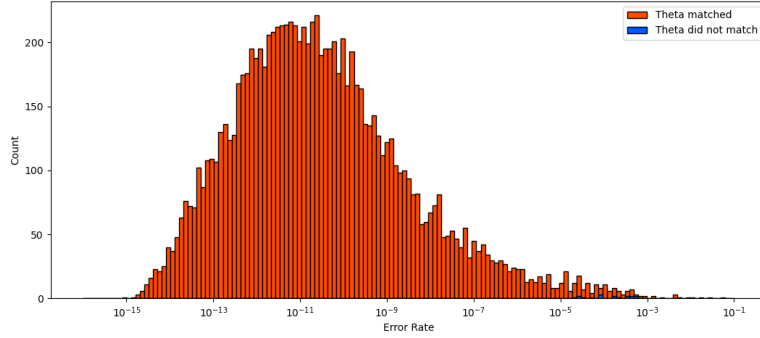


Fig. 3. Distribution of error rates of the solutions

output of Algorithm 1, most of them had an error evaluation function E of 10^{-5} or more. Considering the reproducibility of myCobot, the accuracy of the output of Algorithm 1 cannot be considered good for these samples.

From both the evaluation of the errors in the forward and inverse kinematic solutions, investigating the causes, and proposing solutions for the phenomenon where the output of Algorithm 1 does not match the initially given $\theta_1, \dots, \theta_6$, remains future work.

5 Concluding Remarks

In this paper, we have proposed a solution to the inverse kinematics problem of the 6-DOF manipulator myCobot. The proposed method determines the intersection of the rotation axes for two consecutive joints where the axes intersect. Then, by using the coordinates of the intersection, it derives the rotation angles of each joint. To calculate the rotation axes, we have derived a system of polynomial equations with the coordinates x, y, z of the rotation axes as variables and the position and orientation of the end-effector as parameters within the coefficients. When solving the system of equations, we have computed the CGS of the polynomial system. By avoiding repeated calculations of the Gröbner basis for different positions and orientations, we aim to improve the overall efficiency of the method. In computer experiments, we have demonstrated that the inverse kinematics problem is solved with sufficient accuracy for practical use compared to the size of myCobot.

The challenges of this study are as follows.

First, we need to identify the causes of the inverse kinematics problems that failed to produce correct solutions and to develop appropriate countermeasures. In addition, for cases where the obtained solutions differ from the originally given joint configurations, it is also necessary to investigate the underlying causes and consider suitable remedies.

Second, since the calculation of the CGS is not complete, there are segments that are not covered. One countermeasure is to narrow the parameter space. Due to the structure of myCobot, it may be possible to narrow the parameter space required for solving the inverse kinematics problem. Another countermeasure is to utilize new algorithms or implementations for the CGS [12, 25].

Third, the calculation of trajectory planning using the proposed method. The trajectory planning problem is an extension of the inverse kinematics problem, where the latter involves solving the problem at a single point, while the former requires solving it over an entire given trajectory. In trajectory planning, when there are multiple solutions to the inverse kinematics problem at a certain point on the trajectory, the issue is which solution to choose to move the joints. We have proposed a method that reduces this problem to the shortest path problem in a graph and uses Dijkstra’s algorithm to find the optimal combination of solutions to the inverse kinematic problem [18]. We are currently developing a trajectory planning method that combines the proposed method with this approach [15].

Acknowledgments

The authors would like to thank the anonymous reviewers for their helpful comments. This research is partially supported by JKA and its promotion funds from KEIRIN RACE. In addition, this work was partially supported by the Research Institute for Mathematical Sciences, an International Joint Usage/Research Center located at Kyoto University.

References

1. Denavit, J., Hartenberg, R.: A Kinematic Notation for Lower-Pair Mechanisms Based on Matrices. *Journal of Applied Mechanics* **22**, 215–221 (1955). <https://doi.org/10.1115/1.4011045>
2. Elephant Robotics Co., Ltd.: myCobot 280 M5 (2023), <https://www.elephantrobotics.com/en/mycobot-280-m5-2023-en>, accessed 2025-05-09
3. Faugère, J.C., Merlet, J.P., Rouillier, F.: On solving the direct kinematics problem for parallel robots. Research Report RR-5923, INRIA (2006), <https://hal.inria.fr/inria-00072366>
4. Fukasaku, R., Iwane, H., Sato, Y.: Real Quantifier Elimination by Computation of Comprehensive Gröbner Systems. In: *Proceedings of the 2015 ACM on International Symposium on Symbolic and Algebraic Computation*. pp. 173–180. IS-SAC ’15, ACM, New York, NY, USA (2015). <https://doi.org/10.1145/2755996.2756646>
5. Husty, M.L., Pfurner, M., Schröcker, H.P.: A new and efficient algorithm for the inverse kinematics of a general serial 6R manipulator. *Mech. Mach. Theory* **42.1** pp. 66–81 (2007). <https://doi.org/10.1016/j.mechmachtheory.2006.02.001>
6. Kalker-Kalkman, C.M.: An implementation of Buchbergers’ algorithm with applications to robotics. *Mech. Mach. Theory* **28**(4), 523–537 (1993). [https://doi.org/10.1016/0094-114X\(93\)90033-R](https://doi.org/10.1016/0094-114X(93)90033-R)

7. Kapur, D., Sun, Y., Wang, D.: An efficient method for computing comprehensive Gröbner bases. *J. Symbolic Comput* **52**, 124–142 (2013). <https://doi.org/10.1016/j.jsc.2012.05.015>
8. Kim, C.H., H. R. Kam, S.H.L., Park, T.: RViz: a toolkit for real domain data visualization. In: *Telecommunication Systems*, vol. 60, pp. 337–345. Springer (2015). <https://doi.org/10.1007/s11235-015-0034-5>
9. Macenski, S., Foote, T., Gerkey, B., Lalancette, C., Woodall, W.: Robot Operating System 2: Design, architecture, and uses in the wild. *Science robotics* **7**(66), eabm6074 (2022). <https://doi.org/10.1126/scirobotics.abm6074>
10. Manocha, D., Canny, J.F.: Efficient inverse kinematics for general 6R manipulators. *IEEE Transactions on Robotics and Automation* **10**(5), 648–657 (1994). <https://doi.org/10.1109/70.326569>
11. Nabeshima, K.: CGS: a program for computing comprehensive Gröbner systems in a polynomial ring [computer software] (2018), <https://www.rs.tus.ac.jp/~nabeshima/softwares.html>, accessed 2025-02-05
12. Nabeshima, K.: Generic Gröbner basis of a parametric ideal and its application to a comprehensive Gröbner system. *Appl. Algebra Eng. Commun. Comput.* **35**(1), 55–70 (2024). <https://doi.org/10.1007/S00200-023-00620-8>, <https://doi.org/10.1007/s00200-023-00620-8>
13. Ni, Z., Wu, R.: 6R robot inverse solution algorithm based on quaternion matrix and Gröbner base. *Advances in Linear Algebra & Matrix Theory* **8**(1), 33–40 (2018). <https://doi.org/10.4236/alamt.2018.81004>
14. Noro, M., Takeshima, T.: Risa/Asir — A Computer Algebra System. In: *Proc. ISSAC '92*. pp. 387–396. Association for Computing Machinery, New York, NY, USA (1992). <https://doi.org/10.1145/143242.143362>
15. Okazaki, T., Terui, A., Mikawa, M.: An efficient trajectory planning and an optimized path planning for a 6-Degree-of-Freedom Robot Manipulator. In: *Computer Algebra in Scientific Computing, CASC 2025. Lecture Notes in Computer Science*, Springer (2025), to appear
16. Otaki, S., Terui, A., Mikawa, M.: A Design and an Implementation of an Inverse Kinematics Computation in Robotics Using Real Quantifier Elimination based on Comprehensive Gröbner Systems. Preprint (2021). <https://doi.org/10.48550/arXiv.2111.00384>
17. Pieper, D.L.: The kinematics of manipulators under computer control. Ph.d. thesis, Stanford University (October 1968), <https://apps.dtic.mil/sti/citations/AD0680036>
18. Shirato, Y., Oka, N., Terui, A., Mikawa, M.: An optimized path planning of manipulator with spline curves using real quantifier elimination based on comprehensive gröbner systems. In: *Proceedings of the SCSS 2024 Work in Progress Workshop*. pp. 105–112. Sun SITE Central Europe, RWTH Aachen University (2024), <https://ceur-ws.org/Vol-3754/>
19. Siciliano, B., Sciavicco, L., Villani, L., Oriolo, G.: *Robotics: Modelling, Planning and Control*. Springer (2008). <https://doi.org/10.1007/978-1-84628-642-1>
20. Ricardo Xavier da Silva, S., Schnitman, L., Cesca Filho, V.: A Solution of the Inverse Kinematics Problem for a 7-Degrees-of-Freedom Serial Redundant Manipulator Using Gröbner Bases Theory. *Mathematical Problems in Engineering* **2021**, 6680687 (2021). <https://doi.org/10.1155/2021/6680687>
21. Suzuki, A., Sato, Y.: A simple algorithm to compute comprehensive Gröbner bases using Gröbner bases. In: *Proc. ISSAC 2006*. pp. 326–331 (2006). <https://doi.org/10.1145/1145768.1145821>

22. The PARI Group, Univ. Bordeaux: PARI/GP version 2.13.1 (2021), available from <https://pari.math.u-bordeaux.fr/>
23. Uchida, T., McPhee, J.: Triangularizing kinematic constraint equations using Gröbner bases for real-time dynamic simulation. *Multibody System Dynamics* **25**, 335–356 (2011). <https://doi.org/10.1007/s11044-010-9241-8>
24. Uchida, T., McPhee, J.: Using Gröbner bases to generate efficient kinematic solutions for the dynamic simulation of multi-loop mechanisms. *Mech. Mach. Theory* **52**, 144–157 (2012). <https://doi.org/10.1016/j.mechmachtheory.2012.01.015>
25. Wada, N., Nabeshima, K.: Merging Multiple Algorithms for Computing Comprehensive Gröbner Systems Using Parallel Processing. In: *Computer Algebra in Scientific Computing, CASC 2024. Lecture Notes in Computer Science*, vol. 14938, pp. 373–391. Springer (2024). https://doi.org/10.1007/978-3-031-69070-9_21, https://doi.org/10.1007/978-3-031-69070-9_21
26. Yoshizawa, M., Terui, A., Mikawa, M.: Inverse Kinematics and Path Planning of Manipulator Using Real Quantifier Elimination Based on Comprehensive Gröbner Systems. In: *Computer Algebra in Scientific Computing. CASC 2023, Lecture Notes in Computer Science*, vol. 14139, pp. 393–419. Springer (2023). https://doi.org/10.1007/978-3-031-41724-5_21